Active compounds from a diverse library of triazolothiadiazole and triazolothiadiazine scaffolds: Synthesis, crystal structure determination, cytotoxicity, cholinesterase inhibitor…

ARTICLE *in* BIOORGANIC & MEDICINAL CHEMISTRY · SEPTEMBER 2014

Impact Factor: 2.79 · DOI: 10.1016/j.bmc.2014.08.026

Bioorganic & Medicinal Chemistry xxx (2014) xxx–xxx

Contents lists available at ScienceDirect

Bioorganic & Medicinal Chemistry

journal homepage: www.elsevier.com/locate/bmc

Active compounds from a diverse library of triazolothiadiazole and triazolothiadiazine scaffolds: Synthesis, crystal structure determination, cytotoxicity, cholinesterase inhibitory activity, and binding mode analysis

Imtiaz Khan [a,†], Aliya Ibrar [a], Sumera Zaib [b], Sarfraz Ahmad [b], Norbert Furtmann [c], Shahid Hameed [a,*], Jim Simpson [d], Jürgen Bajorath [c,*], Jamshed Iqbal [b,e,*]

[a] Department of Chemistry, Quaid-i-Azam University, Islamabad 45320, Pakistan
[b] Centre for Advanced Drug Research, COMSATS Institute of Information Technology, Abbottabad 22060, Pakistan
[c] Department of Life Science Informatics, B-IT, LIMES Program Unit Chemical Biology and Medicinal Chemistry, Rheinische Friedrich-Wilhelms-Universität, Dahlmannstr. 2, D-53113 Bonn, Germany
[d] Department of Chemistry, University of Otago, PO Box 56, Dunedin 9054, New Zealand
[e] Department of Pharmaceutical Sciences, COMSATS Institute of Information Technology, Abbottabad 22060, Pakistan

ARTICLE INFO

Article history:
Received 7 August 2014
Revised 21 August 2014
Accepted 22 August 2014
Available online xxxx

Keywords:
Alzheimer's disease
Conjugated heterocycles
X-ray structure
Inhibition
Acetylcholinesterase
Butyrylcholinesterase
Cytotoxicity
Computational analysis

ABSTRACT

In an effort to identify novel cholinesterase candidates for the treatment of Alzheimer's disease (AD), a diverse array of potentially bioactive compounds including triazolothiadiazoles (**4a**–**h** and **5a**–**f**) and triazolothiadiazines (**6a**–**h**) was obtained in good yields through the cyclocondensation reaction of 4-amino-5-(pyridin-3-yl)-4*H*-1,2,4-triazole-3-thiol (**3**) with various substituted aryl/heteroaryl/aryloxy acids and phenacyl bromides, respectively. The structures of newly prepared compounds were confirmed by IR, ^{1}H and ^{13}C NMR spectroscopy and, in case of **4a**, by single crystal X-ray diffraction analysis. The purity of the synthesized compounds was ascertained by elemental analysis. The newly synthesized conjugated heterocycles were screened for cholinesterase inhibitory activity against *electric eel* acetylcholinesterase (EeAChE) and horse serum butyrylcholinesterase (hBChE). Among the evaluated hybrids, several compounds were identified as potent inhibitors. Compounds **5b** and **5d** were most active with an IC_{50} value of 3.09 ± 0.154 and 11.3 ± 0.267 μM, respectively, against acetylcholinesterase, whereas **5b**, **6a** and **6g** were most potent against butyrylcholinesterase, with an IC_{50} of 0.585 ± 0.154, 0.781 ± 0.213, and 1.09 ± 0.156 μM, respectively, compared to neostigmine and donepezil as standard drugs. The synthesized heteroaromatic compounds were also tested for their cytotoxic potential against lung carcinoma (H157) and vero cell lines. Among them, compound **6h** exhibited highest antiproliferative activity against H157 cell lines, with IC_{50} value of 0.96 ± 0.43 μM at 1 mM concentration as compared to vincristine (IC_{50} = 1.03 ± 0.04 μM), standard drug used in this study.

1. Introduction

Alzheimer's disease (AD) is a progressive neurodegenerative disease of the brain, that is, characterized by memory impairment, cognitive dysfunction, and lack of spatial awareness.[1] This devastating neurological disease targets elderly populations and its prevalence is on the rise.[2,3] It is estimated that 24.3 million people worldwide were likely to have Alzheimer's disease (AD) in 2005; also the projected number of individuals with AD all over the world is expected to be on the order 42.3 and 81.1 million by the year 2020 and 2040, respectively.[4] Based on the cholinergic hypothesis, a deficiency of cholinergic neurotransmitters in the basal forebrain might predominantly be involved in Alzheimer's disease. Therefore, augmenting brain cholinergic neurotransmission is thought to be a promising strategy for the inhibition of cholinesterase in the treatment of Alzheimer's disease.[5]

The cholinesterase family comprises acetylcholinesterase (AChE, EC 3.1.1.7) and butyrylcholinesterase (BChE, EC 3.1.1.8),

Abbreviations: AD, Alzheimer's disease; AChE, acetylcholinesterase; BChE, butyrylcholinesterase; ACh, acetylcholine; PAS, peripheral anionic site.

* Corresponding authors. Tel.: +92 51 9064 2133; fax: +92 51 2241 (S.H.); tel.: +92 992 383591/96; fax: +92 992 383441 (J.I.).
E-mail addresses: shameed@qau.edu.pk (S. Hameed), drjamshed@ciit.net.pk (J. Iqbal).
† Present address: School of Chemistry, University of Nottingham, University Park, Nottingham NG7 2RD, UK.

http://dx.doi.org/10.1016/j.bmc.2014.08.026
0968-0896/

which are responsible for the hydrolysis of the neurotransmitter, acetylcholine to choline and acetate, in both the peripheral and central nervous system and this action is known to be one of the most efficient enzyme catalytic reactions.[6] AChE contains five key regions within the active site the consideration of which is required to understand binding patterns of substrate and inhibitors. These regions include (1) catalytic triad residues, (2) the acyl pocket, (3) the oxyanion hole, (4) an anionic site (AS), and (5) a peripheral anionic site (PAS).[7–12] Based on the cholinergic hypothesis, AChE has traditionally been the main target in AD therapy due to its role as the major enzyme to hydrolyze acetyl choline (ACh). So far, BChE has mainly played a supportive role.[13]

In recent years, the search for compounds with AChE and/or BChE inhibitory activity has significantly progressed, particularly since the first cholinesterase inhibitors were officially approved for clinical use in AD therapy. Many of recently reported compounds have been synthesized based on the chemical scaffolds of classical AChE inhibitors including physostigmine, tacrine, galanthamine and donepezil[14] (Fig. 1). Several BChE inhibitors including (−)-cymserine[15] and benzofurans[16] have also been developed. Some other potent and highly selective BChE inhibitors include phenothiazine derivatives such as ethopropazine,[17] *N*-[(2-diethylamino)propionyl]phenothiazine[18] (ASTRA1397), and 10-(9-anthrylcarbonyl)phenothiazine.[19] Hence, the discovery of potent inhibitors of both AChE and BChE is an actively pursued goal in AD treatment.

Heterocyclic compounds occur widely in nature and are essential for life. Nitrogen-containing heterocyclic molecules constitute one of the largest set of chemical entities that are part of many natural products, fine chemicals and biologically active pharmaceuticals.[20] Among them, conjugated heterocycles derived from 1,2,4-triazole scaffold are privileged heterocyclic ring systems featured in a large number of compounds with diverse and important biological profiles. They have drawn strong interest from synthetic as well as medicinal chemists. These hybrid structures have been incorporated into a wide variety of therapeutically important compounds possessing a broad spectrum of biological activities such as antiviral, antifungal, antihelmintic, antitumor, antibacterial, anti-inflammatory, antitubercular, analgesic, antiviral agents and as diuretics, CNS-stimulants, PDE4 inhibitors and hypoglycemic agents.[21–30] Recently, triazolothiadiazoles have been identified as selective inhibitors of the *c*-Met proteins,[31] used as molluscicidal agents,[32] growth promoters,[33] or as acetylcholinesterase, alkaline phosphatase and urease inhibitors.[34]

To further investigate heteroaromatic hybrid structures with a potential to yield new bioactive agents and as part of a larger lead discovery programme[35,36] focusing on cholinesterase inhibitors, we have investigated a library of conjugated heterocycles with promising acetyl- and butyryl-cholinesterase inhibitory activity. The compounds were also tested for their cytotoxic potential. The results of this study are presented herein.

2. Experimental

2.1. General

All commercially available reagents were used as received. Thin layer chromatography (TLC) was performed on Merck DF-Alufoilien 60 F_{254} 0.2 mm precoated plates. Product spots were visualized under UV light at 254 and 365 nm. Melting points were recorded on a Stuart melting point apparatus (SMP3). Infra-red (IR) spectra were recorded on an FTS 3000 MX, Bio-Rad Merlin (Excalibur model) spectrophotometer. NMR spectra were recorded on a Bruker Avance (300 MHz) spectrometer. Chemical shifts (δ) are reported in parts per million (ppm) downfield of tetramethylsilane, using residual solvent signal for spectrum calibration (DMSO-d_6 at 2.50 ppm for ^{1}H and 39.52 ppm for ^{13}C). Abbreviations used in the description of the resonances are: s (singlet), bs (broad singlet), d (doublet), t (triplet), q, (quartet), m (multiplet). The elemental analysis was performed on Leco CHNS-932 Elemental Analyzer, Leco Corporation (USA).

2.2. Synthesis of 4-amino-5-(pyridin-3-yl)-4*H*-1,2,4-triazole-3-thiol (3)

Nicotinohydrazide **1** (1.0 mmol) was stirred with a solution of potassium hydroxide (1.5 mmol) dissolved in methanol (10 mL) at 0–5 °C. Carbon disulfide (1.5 mmol) was added slowly and the reaction mixture left overnight at room temperature. The solid product of potassium dithiocarbazinate **2** was filtered, washed with chilled methanol and dried. It was directly used for the next step without purification.

The potassium dithiocarbazinate **2** was taken in water (8 mL), hydrazine hydrate (2.0 mmol) was added and refluxed for 4–5 h. During the progress of the reaction, the mixture turned green with evolution of hydrogen sulfide and finally it became homogeneous. It was then diluted with little cold water and acidified with conc. hydrochloric acid. The white precipitated solid was filtered,

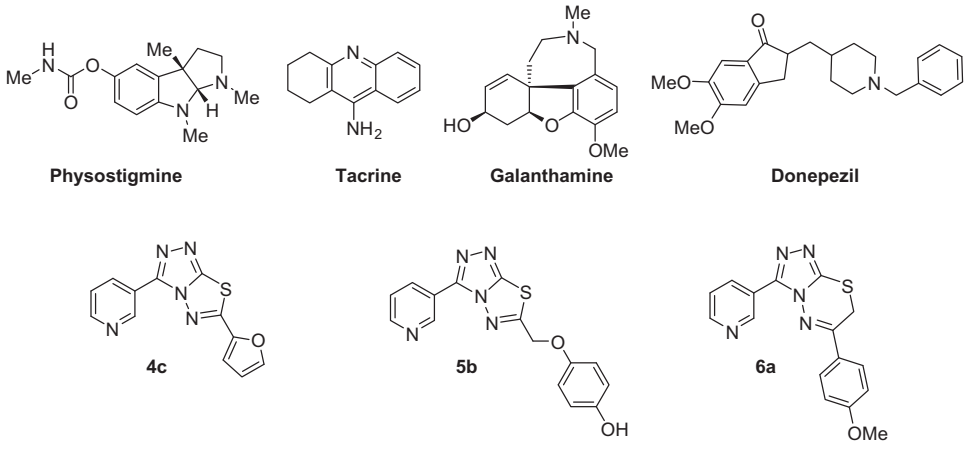

Figure 1. Cholinesterase inhibitors used in AD therapy and synthesized hybrid structures with potent inhibitory activity.

washed with cold water and recrystallized from aqueous methanol yielding product in compliance with literature data.[37]

2.3. Synthesis of 1,2,4-triazolo[3,4-*b*][1,3,4]thiadiazoles (4a–h and 5a–f)

A mixture of 4-amino-5-(pyridin-3-yl)-4*H*-[1,2,4]triazole-3-thiol (**3**) (1.0 mmol) and substituted aromatic acids (1.1 mmol) in $POCl_3$ (5 mL) was refluxed for 6 h. The reaction mixture was slowly poured into crushed ice with stirring and neutralized with sodium bicarbonate. The solid material was filtered, washed with cold water, dried, and recrystallized from ethanol to afford 1,2,4-triazolo[3,4-*b*][1,3,4]thiadiazoles (**4a–h** and **5a–f**).[35]

2.3.1. 6-(4-Chloro-2-fluorophenyl)-3-(pyridin-3-yl)-[1,2,4]triazolo[3,4-*b*][1,3,4]thiadiazole (4a)

Off-white solid (72%, 238 mg): mp 196–197 °C; R_f: 0.68 (10% MeOH/$CHCl_3$); IR (neat, cm^{-1}): 3095 (Ar-H), 1585 (C=N), 1541, 1530 (C=C), 1163 (C—F), 1099 (C—Cl); ^{1}H NMR (300 MHz, DMSO-d_6): δ 9.41 (s, 1H, J = 1.8 Hz, Ar-H), 8.82 (s, 1H, Ar-H), 8.74 (d, 1H, J = 7.4 Hz, Ar-H), 8.60–8.57 (m, 1H, Ar-H), 8.00 (d, 1H, J = 1.5 Hz, Ar-H) 7.66–7.62 (m, 2H, Ar-H), 7.18 (m, 1H, Ar-H); ^{13}C NMR (75 MHz, DMSO-d_6): δ 160.22, 157.41, 154.54, 151.76, 148.65, 146.98, 144.72, 144.49, 142.31, 135.37, 134.64, 132.66, 125.36, 124.53, 122.38, 114.99, 112.91. Anal. Calcd for $C_{14}H_7ClFN_5S$ (331.01): C, 50.68; H, 2.13; N, 21.11; S, 9.67. Found: C, 50.51; H, 2.19; N, 20.98; S, 9.58.

2.3.2. 6-(3-Chloro-4-fluorophenyl)-3-(pyridin-3-yl)-[1,2,4]triazolo[3,4-*b*][1,3,4]thiadiazole (4b)

Off-white solid (77%, 255 mg): mp 210–211 °C; R_f: 0.70 (10% MeOH/$CHCl_3$); IR (neat, cm^{-1}): 3044 (Ar-H), 1594 (C=N), 1576, 1519 (C=C), 1245 (C—F), 970 (C—Cl); ^{1}H NMR (300 MHz, DMSO-d_6): δ 9.41 (s, 1H, Ar-H), 8.74 (d, 1H, J = 7.4 Hz, Ar-H), 8.61 (d, 1H, J = 8.1 Hz, Ar-H), 8.32–8.29 (m, 1H, Ar-H), 8.09–8.04 (m, 1H, Ar-H), 7.68–7.61 (m, 2H, Ar-H); ^{13}C NMR (75 MHz, DMSO-d_6): δ 160.47, 153.75, 151.59, 148.45, 146.24, 145.01, 144.87, 144.49, 143.92, 136.22, 134.98, 132.27, 124.63, 124.02, 122.44, 117.43, 109.51. Anal. Calcd for $C_{14}H_7ClFN_5S$ (331.01): C, 50.68; H, 2.13; N, 21.11; S, 9.67. Found: C, 50.73; H, 2.04; N, 21.08; S, 9.74.

2.3.3. 6-(Furan-2-yl)-3-(pyridin-3-yl)-[1,2,4]triazolo[3,4-*b*][1,3,4]thiadiazole (4c)

Off-white solid (73%, 196 mg): mp 218–219 °C; R_f: 0.66 (10% MeOH/$CHCl_3$); IR (neat, cm^{-1}): 3056 (Ar-H), 1595 (C=N), 1573, 1536 (C=C); ^{1}H NMR (300 MHz, DMSO-d_6): δ 9.39 (s, 1H, Ar-H), 8.75 (d, 1H, J = 6.9 Hz, Ar-H), 8.57–8.53 (m, 1H, Ar-H), 8.15 (d, 1H, J = 0.9 Hz, Ar-H), 7.68–7.63 (m, 2H, Ar-H), 6.88–6.87 (m, 1H, Ar-H); ^{13}C NMR (75 MHz, DMSO-d_6): δ 157.45, 154.57, 151.49, 148.36, 147.00, 144.06, 143.37, 133.66, 124.66, 122.34, 115.90, 113.94. Anal. Calcd for $C_{12}H_7N_5OS$ (269.04): C, 53.52; H, 2.62; N, 26.01; S, 11.91. Found: C, 53.47; H, 2.51; N, 26.12; S, 11.82.

2.3.4. 6-(Furan-3-yl)-3-(pyridin-3-yl)-[1,2,4]triazolo[3,4-*b*][1,3,4]thiadiazole (4d)

Yellow solid (75%, 202 mg): mp 212–213 °C; R_f: 0.69 (10% MeOH/$CHCl_3$); IR (neat, cm^{-1}): 3042 (Ar-H), 1606 (C=N), 1573, 1527 (C=C); ^{1}H NMR (300 MHz, DMSO-d_6): δ 9.42 (d, 1H, J = 1.8 Hz, Ar-H), 8.82 (s, 1H, Ar-H), 8.75 (d, 1H, J = 6.0 Hz, Ar-H), 8.61–8.57 (m, 1H, Ar-H), 8.00 (d, 1H, J = 1.5 Hz, Ar-H), 7.66–7.62 (m, 1H, Ar-H), 7.19–7.18 (m, 1H, Ar-H); ^{13}C NMR (75 MHz, DMSO-d_6): δ 160.27, 154.84, 151.45, 147.01, 146.49, 146.44, 143.92, 133.69, 124.63, 122.40, 117.82, 108.77. Anal. Calcd for $C_{12}H_7N_5OS$ (269.04): C, 53.52; H, 2.62; N, 26.01; S, 11.91. Found: C, 53.41; H, 2.49; N, 25.87; S, 11.79.

2.3.5. 6-(2-Methylfuran-3-yl)-3-(pyridin-3-yl)-[1,2,4]triazolo[3,4-*b*][1,3,4]thiadiazole (4e)

Off-white solid (76%, 215 mg): mp 177–178 °C; R_f: 0.65 (10% MeOH/$CHCl_3$); IR (neat, cm^{-1}): 3081 (Ar-H), 1604 (C=N), 1541, 1505 (C=C); ^{1}H NMR (300 MHz, DMSO-d_6): δ 9.40 (s, 1H, Ar-H), 8.74 (d, 1H, J = 6.6 Hz, Ar-H), 8.58–8.54 (m, 1H, Ar-H), 7.81 (d, 1H, J = 7.2 Hz, Ar-H), 7.67–7.62 (m, 1H, Ar-H), 7.04 (d, 1H, J = 6.8 Hz, Ar-H), 2.68 (s, 3H, CH_3); ^{13}C NMR (75 MHz, DMSO-d_6): δ 161.31, 154.99, 154.74, 151.38, 146.88, 143.75, 143.65, 133.56, 124.68, 122.45, 112.21, 110.27, 14.33. Anal. Calcd for $C_{13}H_9N_5OS$ (283.05): C, 55.11; H, 3.20; N, 24.72; S, 11.32. Found: C, 55.01; H, 3.28; N, 24.65; S, 11.14.

2.3.6. 6-(4-Fluorobenzyl)-3-(pyridin-3-yl)-[1,2,4]triazolo[3,4-*b*][1,3,4]thiadiazole (4f)

Light yellow solid (74%, 230 mg): mp 150–151 °C; R_f: 0.66 (10% MeOH/$CHCl_3$); IR (neat, cm^{-1}): 3064 (Ar-H), 1598 (C=N), 1572, 1505 (C=C), 1220 (C—F); ^{1}H NMR (300 MHz, DMSO-d_6): δ 9.36 (s, 1H, Ar-H), 8.74 (d, 1H, J = 6.8 Hz, Ar-H), 8.54–8.50 (m, 1H, Ar-H), 7.67–7.62 (m, 1H, Ar-H), 7.54–7.49 (m, 2H, Ar-H), 7.26–7.20 (m, 2H, Ar-H), 4.54 (s, 2H, CH_2); ^{13}C NMR (75 MHz, DMSO-d_6): δ 171.42, 163.73, 160.49, 155.72, 151.43, 146.99, 143.61, 133.64, 132.03, 131.99, 131.87, 131.76, 124.64, 122.41, 116.34, 116.05, 36.75. Anal. Calcd for $C_{15}H_{10}FN_5S$ (311.06): C, 57.87; H, 3.24; N, 22.49; S, 11.30. Found: C, 57.61; H, 3.11; N, 22.35; S, 11.17.

2.3.7. 3-(Pyridin-3-yl)-6-(1*H*-pyrrol-2-yl)-[1,2,4]triazolo[3,4-*b*][1,3,4]thiadiazole (4g)

Black solid (71%, 190 mg): mp 189–190 °C; R_f: 0.60 (10% MeOH/$CHCl_3$); IR (neat, cm^{-1}): 3091 (Ar-H), 1604 (C=N), 1580, 1503 (C=C); ^{1}H NMR (300 MHz, DMSO-d_6): δ 12.55 (s, 1H, NH), 9.52 (d, 1H, J = 6.5 Hz, Ar-H), 8.74 (d, 1H, J = 6.9 Hz, Ar-H), 8.68 (d, 1H, J = 8.1 Hz, Ar-H), 7.66–7.24 (m, 2H, Ar-H), 7.02 (d, 1H, J = 6.9 Hz, Ar-H), 6.33–6.27 (m, 1H, Ar-H); ^{13}C NMR (75 MHz, DMSO-d_6): δ 159.57, 154.45, 151.34, 147.00, 143.70, 133.61, 125.83, 124.59, 122.50, 121.00, 115.33, 111.21. Anal. Calcd for $C_{12}H_8N_6S$ (268.05): C, 53.72; H, 3.01; N, 31.32; S, 11.95. Found: C, 53.64; H, 2.89; N, 31.19; S, 11.82.

2.3.8. 6-(4-Ethoxybenzyl)-3-(pyridin-3-yl)-[1,2,4]triazolo[3,4-*b*][1,3,4]thiadiazole (4h)

Brown solid (74%, 249 mg): mp 194–195 °C; R_f: 0.69 (10% MeOH/$CHCl_3$); IR (neat, cm^{-1}): 3029 (Ar-H), 1601 (C=N), 1582, 1510 (C=C); ^{1}H NMR (300 MHz, DMSO-d_6): δ 8.81 (d, 2H, J = 6.8 Hz, Ar-H), 8.14 (d, 2H, J = 6.8 Hz, Ar-H), 7.35 (d, 2H, J = 8.1 Hz, Ar-H), 6.93 (d, 2H, J = 8.4 Hz, Ar-H), 4.45 (s, 2H, CH_2), 4.02 (q, 2H, J = 6.9 Hz, CH_2), 1.30 (t, 3H, J = 6.9 Hz, CH_3); ^{13}C NMR (75 MHz, DMSO-d_6): δ 172.40, 158.55, 155.68, 151.42, 147.00, 146.54, 143.50, 133.64, 130.95, 127.40, 124.64, 115.26, 63.50, 36.86, 15.08. Anal. Calcd for $C_{17}H_{15}N_5OS$ (337.10): C, 60.52; H, 4.48; N, 20.76; S, 9.50. Found: C, 60.43; H, 4.34; N, 20.59; S, 9.38.

2.3.9. 2-((3-(Pyridin-3-yl)-[1,2,4]triazolo[3,4-*b*][1,3,4]thiadiazol-6-yl)methoxy)phenol (5a)

Light yellow solid (70%, 227 mg): mp 211–212 °C; R_f: 0.67 (10% MeOH/$CHCl_3$); IR (neat, cm^{-1}): 3225 (OH), 3030 (Ar-H), 1567 (C=N), 1513, 1501 (C=C); ^{1}H NMR (300 MHz, DMSO-d_6): δ 9.14 (d, 1H, J = 1.5 Hz, Ar-H), 8.71 (d, 1H, J = 6.0 Hz, Ar-H), 8.38 (d, 1H, J = 8.1 Hz, Ar-H), 7.60–7.44 (m, 1H, Ar-H), 6.87–6.75 (m, 3H, Ar-H), 6.69–6.64 (m, 1H, Ar-H), 5.83 (s, 1H, OH), 4.34 (s, 2H, OCH_2); ^{13}C NMR (75 MHz, DMSO-d_6): δ 173.01, 167.71, 151.53, 149.82, 148.98, 148.20, 148.15, 136.05, 124.04, 123.64, 122.60, 119.28, 118.91, 117.14, 70.80. Anal. Calcd for $C_{15}H_{11}N_5O_2S$ (325.06): C, 55.38; H, 3.41; N, 21.53; S, 9.86. Found: C, 55.26; H, 3.29; N, 21.42; S, 9.95.

2.3.10. 4-((3-(Pyridin-3-yl)-[1,2,4]triazolo[3,4-*b*][1,3,4]thiadiazol-6-yl)methoxy)phenol (5b)

Light yellow solid (72%, 234 mg): mp 230–231 °C; R_f: 0.68 (10% MeOH/$CHCl_3$); IR (neat, cm^{-1}): 3113 (OH), 3024 (Ar-H), 1620 (C═N), 1554, 1502 (C═C); ^1H NMR (300 MHz, DMSO-d_6): δ 9.34 (d, 1H, J = 1.8 Hz, Ar-H), 8.75–8.73 (m, 1H, Ar-H), 8.53–8.49 (m, 1H, Ar-H), 7.68–7.60 (d, 1H, Ar-H), 7.13–7.02 (m, 4H, Ar-H), 5.59 (s, 3H, OH, CH_2); ^{13}C NMR (75 MHz, DMSO-d_6): δ 173.01, 169.27, 155.33, 151.51, 146.97, 143.76, 133.69, 124.69, 123.64, 122.69, 121.65, 116.38, 65.85. Anal. Calcd for $C_{15}H_{11}N_5O_2S$ (325.06): C, 55.38; H, 3.41; N, 21.53; S, 9.86. Found: C, 55.24; H, 3.26; N, 21.62; S, 9.67.

2.3.11. 3-(Pyridin-3-yl)-6-(*o*-tolyloxymethyl)-[1,2,4]triazolo[3,4-*b*][1,3,4]thiadiazole (5c)

Brown solid (78%, 252 mg): mp 180–181 °C; R_f: 0.69 (10% MeOH/$CHCl_3$); IR (neat, cm^{-1}): 3052 (Ar-H), 1590 (C═N), 1572, 1494 (C═C); ^1H NMR (300 MHz, DMSO-d_6): δ 9.36 (s, 1H, Ar-H), 8.74 (d, 1H, J = 6.0 Hz, Ar-H), 8.52 (d, 1H, J = 8.1 Hz, Ar-H), 7.67–7.63 (m, 1H, Ar-H), 7.23–7.12 (m, 3H, Ar-H), 6.94 (t, 1H, J = 7.2 Hz, Ar-H), 5.63 (s, 1H, OCH_2), 2.26 (s, 3H, CH_3); ^{13}C NMR (75 MHz, DMSO-d_6): δ 169.59, 155.59, 155.26, 151.51, 146.97, 143.75, 133.62, 131.28, 127.62, 126.56, 124.65, 122.30, 112.67, 65.37, 16.37. Anal. Calcd for $C_{16}H_{13}N_5OS$ (323.08): C, 59.43; H, 4.05; N, 21.66; S, 9.92. Found: C, 59.25; H, 4.01; N, 21.57; S, 9.79.

2.3.12. 3-(Pyridin-3-yl)-6-(*p*-tolyloxymethyl)-[1,2,4]triazolo[3,4-*b*][1,3,4]thiadiazole (5d)

Light brown solid (76%, 245 mg): mp 184–185 °C; R_f: 0.66 (10% MeOH/$CHCl_3$); IR (neat, cm^{-1}): 3059 (Ar-H), 1609 (C═N), 1588, 1511 (C═C); ^1H NMR (300 MHz, DMSO-d_6): δ 9.36 (s, 1H, Ar-H), 8.75 (d, 1H, J = 6.0 Hz, Ar-H), 8.53–8.49 (m, 1H, Ar-H), 7.67–7.63 (m, 1H, Ar-H), 7.14 (d, 2H, J = 8.4 Hz, Ar-H), 7.02 (d, 2H, J = 8.7 Hz, Ar-H), 5.59 (s, 2H, OCH_2), 2.24 (s, 3H, CH_3); ^{13}C NMR (75 MHz, DMSO-d_6): δ 169.34, 155.40, 155.33, 151.51, 146.97, 143.75, 133.64, 131.48, 130.54, 124.66, 122.28, 115.40, 65.39, 20.55. Anal. Calcd for $C_{16}H_{13}N_5OS$ (323.08): C, 59.43; H, 4.05; N, 21.66; S, 9.92. Found: C, 59.37; H, 4.14; N, 21.48; S, 9.76.

2.3.13. 6-((4-Methoxyphenoxy)methyl)-3-(pyridin-3-yl)-[1,2,4]triazolo[3,4-*b*][1,3,4] thiadiazole (5e)

Light brown solid (75%, 254 mg): mp 170–171 °C; R_f: 0.68 (10% MeOH/$CHCl_3$); IR (neat, cm^{-1}): 3063 (Ar-H), 1596 (C═N), 1573, 1507 (C═C); ^1H NMR (300 MHz, DMSO-d_6): δ 9.35 (d, 1H, J = 1.5 Hz, Ar-H), 8.75–8.73 (m, 1H, Ar-H), 8.53–8.49 (m, 1H, Ar-H), 7.67–7.63 (m, 1H, Ar-H), 7.11–7.05 (m, 2H, Ar-H), 6.93–6.88 (m, 2H, Ar-H), 5.56 (s, 2H, OCH_2), 3.70 (s, 3H, OCH_3); ^{13}C NMR (75 MHz, DMSO-d_6): δ 169.44, 155.33, 154.94, 151.52, 151.44, 146.99, 143.76, 133.65, 124.65, 122.29, 116.77, 115.23, 66.01, 55.85. Anal. Calcd for $C_{16}H_{13}N_5O_2S$ (330.08): C, 56.63; H, 3.86; N, 20.64; S, 9.45. Found: C, 56.49; H, 4.02; N, 20.57; S, 9.54.

2.3.14. 6-((4-Fluorophenoxy)methyl)-3-(pyridin-3-yl)-[1,2,4]triazolo[3,4-*b*][1,3,4]thiadiazole (5f)

Light brown solid (77%, 252 mg): mp 176–177 °C; R_f: 0.65 (10% MeOH/$CHCl_3$); IR (neat, cm^{-1}): 3042 (Ar-H), 1597 (C═N), 1573, 1503 (C═C), 1192 (C—F); ^1H NMR (300 MHz, DMSO-d_6): δ 9.35 (s, 1H, Ar-H), 8.74 (d, 1H, J = 6.0 Hz, Ar-H), 8.52–8.49 (m, 1H, Ar-H), 7.66–7.62 (m, 1H, Ar-H), 7.19–7.16 (m, 4H, Ar-H), 5.62 (s, 2H, OCH_2); ^{13}C NMR (75 MHz, DMSO-d_6): δ 168.86, 159.40, 156.25, 155.34, 155.83, 153.80, 151.51, 146.97, 143.76, 133.62, 124.62, 122.26, 117.19, 117.09, 116.77, 116.46, 65.94. Anal. Calcd for $C_{15}H_{10}FN_5OS$ (327.06): C, 55.04; H, 3.08; N, 21.39; S, 9.80. Found: C, 54.91; H, 2.98; N, 21.25; S, 9.68.

2.4. Synthesis of 1,2,4-triazolo[3,4-*b*][1,3,4]-thiadiazines (6a–h)

A mixture of 4-amino-5-(pyridin-3-yl)-4*H*-[1,2,4]triazole-3-thiol (**3**) (1.0 mmol) and substituted phenacyl bromides (1.2 mmol) was refluxed in absolute ethanol (10 mL) for 7 h. The reaction mass was poured into crushed ice and neutralized with sodium bicarbonate. The solid product obtained was filtered, washed with water, dried and recrystallized from ethanol to afford thiadiazines **6a**–**h**.[38] The data for compounds **6a** and **6d** was found to be consistent with the literature values.[39]

2.4.1. 6-(4-Chlorophenyl)-3-(pyridin-3-yl)-7*H*-[1,2,4]triazolo[3,4-*b*][1,3,4]thiadiazine (6b)

Off-white solid (79%, 258 mg): mp 246–247 °C; R_f: 0.61 (10% MeOH/$CHCl_3$); IR (neat, cm^{-1}): 3036 (Ar-H), 2856, 2833 (CH_2), 1635 (C═N), 1584, 1505 (C═C), 1091 (C—Cl); ^1H NMR (300 MHz, DMSO-d_6): δ 9.30 (s, 1H, Ar-H), 8.90 (d, 1H, J = 3.3 Hz, Ar-H), 8.69 (d, 1H, J = 8.1 Hz, Ar-H), 8.06 (d, 2H, J = 8.7 Hz, Ar-H), 7.94–7.92 (m, 1H, Ar-H), 7.67 (d, 2H, J = 8.4 Hz, Ar-H), 4.48 (s, 2H, SCH_2); ^{13}C NMR (75 MHz, DMSO-d_6): δ 156.75, 149.24, 148.55, 146.77, 143.98, 137.46, 135.72, 132.73, 131.14, 128.54, 126.07, 125.48, 21.47. Anal. Calcd for $C_{15}H_{10}ClN_5S$ (327.03): C, 54.96; H, 3.07; N, 21.37; S, 9.78. Found: C, 54.85; H, 3.17; N, 21.20; S, 9.65.

2.4.2. 6-(4-Fluorophenyl)-3-(pyridin-3-yl)-7*H*-[1,2,4]triazolo[3,4-*b*][1,3,4]thiadiazine (6c)

Off-white solid (82%, 255 mg): mp 232–233 °C; R_f: 0.57 (10% MeOH/$CHCl_3$); IR (neat, cm^{-1}): 3054 (Ar-H), 2857, 2842 (CH_2), 1598 (C═N), 1572, 1511 (C═C), 1220 (C—F); ^1H NMR (300 MHz, DMSO-d_6): δ 9.21 (d, 1H, J = 1.2 Hz, Ar-H), 8.79–8.78 (m, 1H, Ar-H), 8.47 (d, 1H, J = 7.8 Hz, Ar-H), 8.12–8.07 (m, 2H, Ar-H), 7.74–7.70 (m, 1H, Ar-H), 7.47–7.41 (m, 2H, Ar-H), 4.47 (s, 2H, SCH_2); ^{13}C NMR (75 MHz, DMSO-d_6): δ 166.50, 163.17, 156.00, 150.35, 149.74, 147.78, 143.58, 136.89, 130.86, 130.74, 130.29, 130.25, 124.88, 123.12, 116.92, 116.62, 23.40. Anal. Calcd for $C_{15}H_{10}FN_5S$ (311.06): C, 57.87; H, 3.24; N, 22.49; S, 10.30. Found: C, 57.74; H, 3.11; N, 22.61; S, 10.14.

2.4.3. 6-(4-Biphenyl)-3-(pyridin-3-yl)-7*H*-[1,2,4]triazolo[3,4-*b*][1,3,4]thiadiazine (6e)

Light yellow solid (78%, 288 mg): mp 204–205 °C; R_f: 0.59 (10% MeOH/$CHCl_3$); IR (neat, cm^{-1}): 3026 (Ar-H), 2969, 2865 (CH_2), 1604 (C═N), 1572, 1506 (C═C); ^1H NMR (300 MHz, DMSO-d_6): δ 9.35 (s, 1H, Ar-H), 8.93–8.91 (m, 1H, Ar-H), 8.77 (d, 1H, J = 8.1 Hz, Ar-H), 8.14 (d, 2H, J = 8.4 Hz, Ar-H), 7.99–7.95 (m, 1H, Ar-H), 7.91 (d, 2H, J = 8.4 Hz, Ar-H), 7.78 (d, 2H, J = 7.5 Hz, Ar-H), 7.54–7.49 (m, 2H, Ar-H), 7.43 (t, 1H, J = 7.2 Hz, Ar-H), 4.53 (s, 2H, SCH_2); ^{13}C NMR (75 MHz, DMSO-d_6): δ 156.85, 148.88, 147.76, 145.25, 144.13, 144.10, 139.76, 139.16, 132.46, 129.61, 128.88, 127.73, 127.38, 126.17, 124.16, 23.43. Anal. Calcd for $C_{21}H_{15}N_5S$ (369.10): C, 68.27; H, 4.09; N, 18.96; S, 8.68. Found: C, 68.11; H, 4.02; N, 18.99; S, 8.51.

2.4.4. 6-(Naphthalen-1-yl)-3-(pyridin-3-yl)-7*H*-[1,2,4]triazolo[3,4-*b*][1,3,4]thiadiazine (6f)

Off-white solid (82%, 281 mg): mp 275–276 °C; R_f: 0.55 (10% MeOH/$CHCl_3$); IR (neat, cm^{-1}): 3038 (Ar-H), 2878, 2832 (CH_2), 1627 (C═N), 1591, 1549 (C═C); ^1H NMR (300 MHz, DMSO-d_6): δ 9.39 (s, 1H, J = 1.2 Hz, Ar-H), 8.96 (d, 1H, J = 4.2 Hz, Ar-H), 8.83 (d, 1H, J = 8.1 Hz, Ar-H), 8.71 (bs, 1H, Ar-H), 8.16–7.99 (m, 5H, Ar-H), 7.70–7.63 (m, 2H, Ar-H), 4.64 (s, 2H, SCH_2); ^{13}C NMR (75 MHz, DMSO-d_6): δ 157.09, 148.78, 147.33, 144.81, 144.24, 140.20, 134.85, 132.86, 130.82, 130.10, 129.53, 129.37, 128.99, 128.24, 127.74, 126.40, 124.32, 123.71, 23.39. Anal. Calcd for $C_{19}H_{13}N_5S$ (343.09): C, 66.45; H, 3.82; N, 20.39; S, 9.34. Found: C, 66.30; H, 3.67; N, 20.24; S, 9.42.

Please cite this article in press as: Khan, I.; et al. *Bioorg. Med. Chem.* (2014), http://dx.doi.org/10.1016/j.bmc.2014.08.026

2.4.5. 6-(4-Nitrophenyl)-3-(pyridin-3-yl)-7*H*-[1,2,4]triazolo[3,4-*b*][1,3,4]thiadiazine (6g)

Yellow solid (77%, 260 mg): mp 234–235 °C; R_f: 0.56 (10% MeOH/$CHCl_3$); IR (neat, cm^{-1}): 3056 (Ar-H), 2967, 2927 (CH_2), 1597 (C=N), 1577, 1513 (C=C) 1453, 1347 (C-NO_2); ^{1}H NMR (300 MHz, DMSO-d_6): δ 9.20 (s, 1H, Ar-H), 8.81 (d, 1H, J = 4.5 Hz, Ar-H), 8.50–8.46 (m, 1H, Ar-H), 8.45–8.39 (m, 2H, Ar-H), 8.26 (d, 2H, J = 9.0 Hz, Ar-H), 7.76–7.71 (m, 1H, Ar-H), 4.54 (s, 2H, SCH_2); ^{13}C NMR (75 MHz, DMSO-d_6): δ 155.32, 150.34, 149.94, 149.70, 147.70, 143.56, 139.66, 137.15, 129.52, 124.99, 124.61, 123.01, 23.56. Anal. Calcd for $C_{15}H_{10}N_6O_2S$ (338.06): C, 53.25; H, 2.98; N, 24.84; S, 9.48. Found: C, 53.09; H, 2.84; N, 24.72; S, 9.38.

2.4.6. 6-(3,4-Dichlorophenyl)-3-(pyridin-3-yl)-7*H*-[1,2,4]triazolo[3,4-*b*][1,3,4]thiadiazine (6h)

Light yellow solid (81%, 293 mg): mp 242–243 °C; R_f: 0.53 (10% MeOH/$CHCl_3$); IR (neat, cm^{-1}): 3015 (Ar-H), 2918, 2854 (CH_2), 1635 (C=N), 1591, 1546 (C=C), 1025 (C—Cl); ^{1}H NMR (300 MHz, DMSO-d_6): δ 9.24 (s, 1H, Ar-H), 8.85 (d, 1H, J = 4.5 Hz, Ar-H), 8.58 (d, 1H, J = 8.1 Hz, Ar-H), 8.26 (d, 1H, J = 2.1 Hz, Ar-H), 8.01–7.98 (m, 1H, Ar-H), 7.88–7.81 (m, 2H, Ar-H), 4.48 (s, 2H, SCH_2); ^{13}C NMR (75 MHz, DMSO-d_6): δ 155.13, 149.47, 149.21, 146.62, 143.78, 138.34, 135.35, 134.28, 132.57, 131.85, 130.07, 128.13, 125.51, 123.46, 23.40. Anal. Calcd for $C_{15}H_9Cl_2N_5S$ (361.00): C, 49.74; H, 2.50; N, 19.33; S, 8.85. Found: C, 49.63; H, 2.36; N, 19.39; S, 8.74.

2.5. Pharmacological assays

2.5.1. Cholinesterase inhibition assay

Ellman's method[40] was used to evaluate the inhibitory activities of the synthesized compounds against EeAChE and hBChE. The compounds were first dissolved in DMSO (end concentration of DMSO was 1% in the assay) and studied at a 0.5 mM final concentration for initial screening. The compounds exhibiting more than 50% inhibition were further tested using eight to ten serial dilutions in assay buffer (50 mM Tris–HCl, 0.1 M NaCl and 0.02 M $MgCl_2$, pH 8.0). Composition of the reaction mixture was: 20 μL assay buffer, 10 μL of test compound and 10 μL of enzymes (0.5 and 3.4 U/mg of EeAChE or hBChE, respectively). A 10 min pre-incubation of the reaction mixture at 25 °C was carried out. At the end of the pre-incubation period, 10 μL of 1 mM acetylthiocholine iodide or butyrylthiocholine chloride were added to the respective EeAChE or hBChE enzyme solution to start the enzymatic reactions. The mixtures were incubated for 15 min at 25 °C. The change in the absorbance was measured at 405 nm to determine the amount of the product using a microplate reader (Bio-Tek ELx800™). Neostigmine and donepezil were used as standard inhibitors. Assays were performed with a blank containing all of the components except enzyme or substrate in order to account for a non-enzymatic reaction. Each concentration was analyzed in triplicate. The enzyme dilution buffer consisted of 50 mM Tris–HCl buffer containing 0.1% (w/v) bovine serum albumin (BSA) and pH 8.0. The linear regression parameters were determined for each curve and the IC_{50} values were measured. The computer program GraphPad Prism 5.0 (San Diego, CA, USA) was used to analyse the data.

2.5.2. Cytotoxicity

2.5.2.1. Cell lines and cultures. Lung carcinoma (H157), and African green monkey kidney normal cell line (Vero), were kept in RPMI-1640 [having heat-inactivated fetal bovine serum (10%), glutamine (2 mM), Pyruvate (1 mM), 100 U/mL penicillin and 100 μg/mL streptomycin] in T-75 cm^2 sterile tissue culture flasks in a 5% CO_2 incubator at 37 °C.[41] 96-well plates were used for growing H157 and Vero cells by inoculating 10^4 cells per 100 μL per well. For experiments, cell lines were grown in 96-well plates by inoculating 5×10^4 cells/100 μL/well respectively, and plates were incubated at 37 °C in a 5% CO_2 incubator. Within 24 h, a uniform monolayer was formed which was used for experiments.

2.5.2.2. Cytotoxicity analysis by sulforhodamine B (SRB) assay. To perform cytotoxicity assay with H157 and Vero cells, a previously described method by Skehan et al.[42] was adopted with some modifications. Briefly, cells were cultured in different 96 well plates for 24 h. The compounds in different concentrations (100, 10, 1 and 0.1 μM) were inoculated in test wells while control and blank wells were also prepared contain standard drug (VCN) and culture media with cells, respectively. The plates were then incubated for 48 h. After that cells were fixed with 50 μL of 50% ice cold TCA solution at 4 °C for 1 h. The plates were washed 5 times with PBS and air dried. Fixed cells were further treated with 0.4% w/v sulforhodamine B dye prepared in 1% acetic acid solution and left at room temperature for 30 min. After that the plates were rinsed with 1% acetic acid solution and allowed to dry. In order to solubilize the dye, the dried plates were treated with 10 mM Tris base solution for 10 min at room temperature. Absorbance was measured at 490 nm subtracting the background measurement at 630 nm.[43]

2.6. X-ray structure determination

Diffraction data were collected on a Bruker APEXII CCD diffractometer using Mo-Kα (λ = 0.71073 Å) at ~90 K. Each crystal was mounted on a mylar loop in a thin film of Paratone N oil. A full sphere of data was collected using the ω-scan technique. Data were processed with APEX2 and SAINT[44] with multi-scan absorption corrections applied using SADABS.[44] The structures were solved with SHELXS[45] and refined using SHELXL[45] and TITAN.[46] All non-hydrogen atoms were assigned anisotropic displacement parameters, with hydrogen atoms included in calculated positions. Crystals were only weakly diffracting. The best diffraction pattern obtained in three attempts using 60 s scans for each frame recorded was used. However, despite weak diffraction, the structure was readily solved and refined to high resolution. The molecular plot and the packing diagram were produced using Mercury.[47]

2.7. Computational binding mode analysis

The X-ray structures of human AChE (PDB ID 4BDT)[48] in complex huprine W and of human BChE (PDB ID 4BDS)[48] bound to tacrine were obtained from the RCSB Protein Bank[49] and used as templates for flexible ligand docking with AutoDock 4.2.[50] The side chain of residue Tyr337 in the active site of AChE was also treated flexibly during docking while all other residues were fixed in their crystallographic conformation. For BChE, where residue Ala328 replaces Tyr337 in AChE, the entire active site was kept rigid. Prior to the calculations, crystallographic water and ligand molecules were removed from the template structures and hydrogen atoms were added using the Molecular Operating Environment (MOE 2012.10).[51] Atomic partial charges were added with AutoDock Tools.[50] The best dual AChE/BChE inhibitor **5b** was docked into the active sites of AChE and BChE using the Lamarckian Genetic Algorithm in AutoDock 4.2. Putative compound binding modes were selected by visual inspection of high-scoring docking poses.

3. Results and discussion

3.1. Chemistry

The reaction sequences employed for compound synthesis are illustrated in Scheme 1. The starting material nicotinohydrazide

(**1**) reacting with carbon disulfide in methanolic potassium hydroxide produced the corresponding dithiocarbazinate (**2**) in good yield. The salt **2** was used directly for the next step without further purification.

4-Amino-5-(pyridin-3-yl)-4*H*-1,2,4-triazole-3-thiol (**3**) was synthesized by refluxing **2** with hydrazine hydrate (80%).[37] Formation of the triazole **3** was indicated in its IR spectrum where absorption bands were observed at 3226, 2565 and 1602 cm^{-1} due to —NH_2, —SH, and —C=N, respectively. Its ^1H NMR spectrum exhibited two singlets at 14.08 and 5.82 ppm ascribable to the —SH and —NH_2 protons, respectively. Condensation of triazole **3** with various aromatic/heteroaromatic carboxylic acids in phosphorous oxychloride under reflux produced a diverse array of 1,2,4-triazolo [3,4-*b*][1,3,4]thiadiazoles (**4a**–**h** and **5a**–**f**).[35] A wide range of substituents including various electron-donating as well as electron-withdrawing groups on aryl ring have been tolerated resulting in condensed frameworks in ample yields. The cyclocondensation reaction was also found to be compatible with heteroaromatic motifs like 2-furanyl, 3-furanyl as well as 2-pyrrolyl, providing access to the desired products. The appearance of new stretching bands in the IR spectra for —C=N and disappearance of characteristic peaks for —SH and —NH_2 groups clearly indicated successful cyclization. In the ^1H NMR spectra of compounds **5a**–**f**, signals observed in the range of 5.63–4.34 ppm as singlets for methylene protons confirmed the formation of triazolothiadiazoles. On the other hand, the condensation of triazole (**3**) with various phenacyl bromides in absolute ethanol under reflux resulted in the formation of 6-(aryl)-3-(pyridin-4-yl)-7*H*-[1,2,4]triazolo[3,4-*b*][1,3,4]thiadiazines (**6a**–**h**)[38] in good yields. Reactions of substrates with both electron-rich as well as electron-deficient groups on the aryl ring proceeded smoothly under standard reaction conditions. The phenacyl bromides with bulky aryl groups including biphenyl and naphthyl were also found to be effective coupling partners in this cyclization reaction producing triazolothiadiazines in high yields. These structures were confirmed through ^1H NMR spectroscopy where signals observed in the range of 4.64–4.44 ppm were assigned to the —SCH_2 group of triazolothiadiazines. ^{13}C NMR spectra of condensed heterocycles (**6a**–**h**) showed the presence of carbon signals in the range of 23.56–21.47 ppm attributed to the —SCH_2 group. The formula of newly synthesized compounds and their purity was ascertained by elemental analysis.

The molecular structure of **4a** was determined by X-ray crystallography. The crystal and instrumental parameters used in the unit cell determination, the data collection, and structure refinement parameters are presented in Table 1. Selected bond distances and angles are reported in Table 2. The structure comprises a central [1,2,4]triazolo[3,4-*b*][1,3,4]thiadiazole unit substituted in the 3-position by a pyridine ring and with a 4-chloro-2-fluorophenyl substituent on the C atom of the thiadiazole ring (Fig. 2). The entire molecule is close to being planar with an rms deviation of only 0.062 Å from the best-fit mean plane through all 20 non-hydrogen atoms in the molecule.

An intramolecular C8—H8...N4 hydrogen bond further supports the planarity of the molecular structure. In keeping with this the dihedral angle between the triazole and thiadiazole rings of the [1,2,4]triazolo[3,4-*b*][1,3,4]thiadiazole unit is 1.33(9)° while the [1,2,4]triazolo[3,4-*b*][1,3,4]thiadiazole unit subtends angles of 4.53(6)° and 5.07(6)° to the pyridine and chlorofluorophenyl rings, respectively. The Cambridge Structural Database[52] revealed 14 structures of 6-phenyl-substituted-[1,2,4]triazolo[3,4-*b*][1,3,4]thiadiazoles, but no structures of molecules with pyridine substitution in the 3-position have been reported.

C—H...N hydrogen bonds form layers approximately parallel to [1 0 2] while short N5...S1 [2.8091 (19) Å] and Cl1...Cl1 [3.4732 (11) Å] contacts are also found and contribute to the overall stability of the layers. Cg...Cg contacts involving all four aromatic rings in the structure with centroid...centroid distances in the range 3.3119(11) Å to 3.7825(12) Å stack the layers along the *c* axis (Fig. 3).

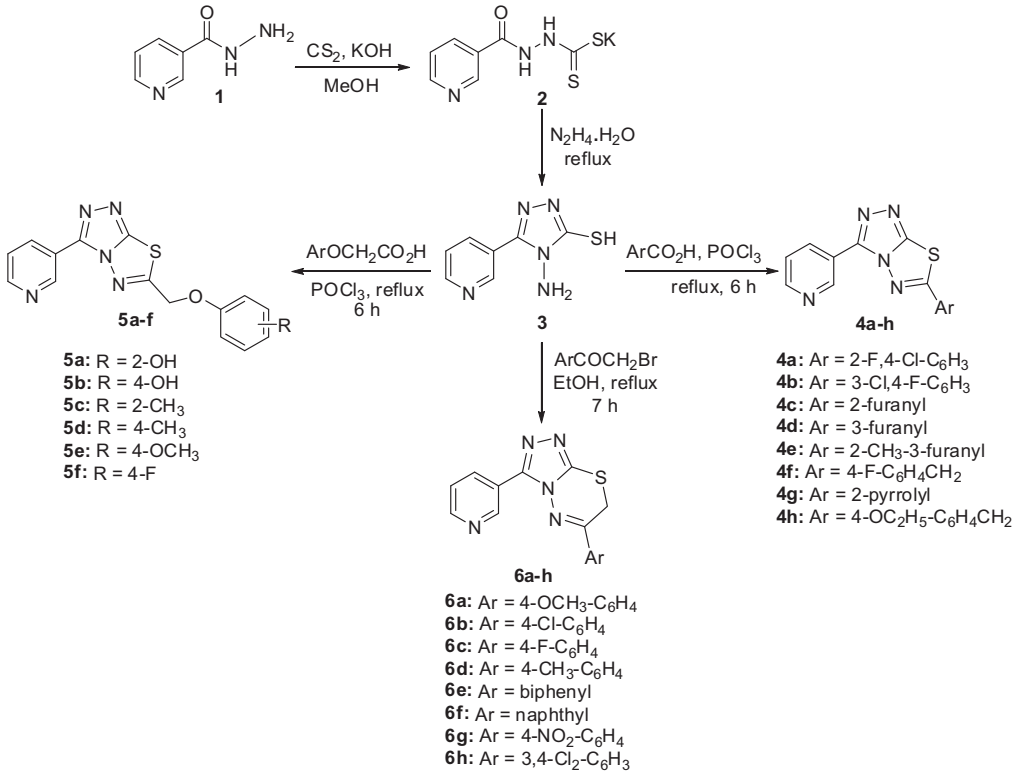

Scheme 1. Synthetic protocol for compounds **4a**–**h**, **5a**–**f** and **6a**–**h**.

Table 1
Crystal data and structure refinement for **4a**

Empirical formula	$C_{14}H_7N_5ClFS$
Formula weight	331.76
Temperature	91(2) K
Wavelength	0.71073 Å
Crystal system	Monoclinic
Space group	$P\,21/c$
Unit cell dimensions	$a = 13.1456(4)$ Å, $\alpha = 90°$ $b = 14.5535(5)$ Å, $\beta = 105.683(2)°$ $c = 7.3446(2)$ Å, $\gamma = 90°$
Volume	1352.82(7) Å^3
Z	4
Density (calculated)	1.629 mg/m^3
Absorption coefficient	0.451 mm^{-1}
$F(000)$	672
Crystal size	0.30 × 0.28 × 0.10 mm^3
Theta range for data collection	2.80 to 32.45°
Index ranges	−19<=h<=19, −16<=k<=21, −10<=l<=10
Reflections collected	17393
Independent reflections	3652 [R(int) = 0.0561]
Completeness to theta = 32.45°	74.9%
Absorption correction	Semi-empirical from equivalents
Max. and min. transmission	1.000 and 0.806
Refinement method	Full-matrix least-squares on F^2
Data/restraints/parameters	3652/0/199
Goodness-of-fit on F^2	1.044
Final R indices [$I > 2\sigma(I)$]	$R_1 = 0.0463$, w$R_2 = 0.1289$
R indices (all data)	$R_1 = 0.0674$, w$R_2 = 0.1358$
Largest diff. peak and hole	0.525 and −0.503 e Å^{-3}
CCDC	994768

Table 2
Selected bond lengths (Å) and angles (°) for **4a**

Bond lengths (Å)			
N(1)—C(1)	1.326(3)	C(4)—C(8)	1.401(3)
N(1)—N(2)	1.400(2)	N(5)—C(8)	1.333(3)
N(2)—C(3)	1.318(3)	N(5)—C(7)	1.336(3)
C(1)—N(3)	1.362(3)	C(2)—C(9)	1.467(3)
N(3)—N(4)	1.365(2)	C(12)—Cl(1)	1.736(2)
N(3)—C(3)	1.368(3)	C(12)—C(13)	1.389(3)
N(4)—C(2)	1.296(3)	C(13)—C(14)	1.380(3)
C(2)—S(1)	1.767(2)	C(9)—C(14)	1.386(3)
S(1)—C(3)	1.732(2)	C(14)—F(1)	1.356(2)
C(1)—C(4)	1.461(3)		
Bond angles (°)			
C(1)—N(1)—N(2)	109.31(17)	N(4)—C(2)—C(9)	118.59(18)
C(3)—N(2)—N(1)	105.29(16)	N(4)—C(2)—S(1)	117.11(15)
N(1)—C(1)—N(3)	108.12(18)	C(3)—S(1)—C(2)	87.48(10)
C(1)—N(3)—N(4)	134.77(18)	C(9)—C(2)—S(1)	124.27(15)
C(1)—N(3)—C(3)	106.39(17)	N(1)—C(1)—C(4)	126.5(2)
N(4)—N(3)—C(3)	118.82(18)	N(3)—C(1)—C(4)	125.40(18)
C(2)—N(4)—N(3)	107.69(17)		

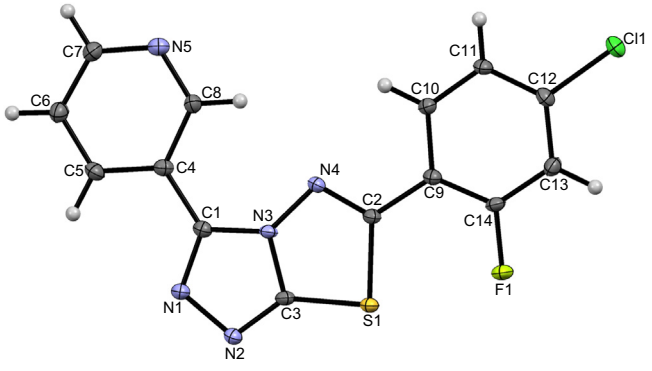

Figure 2. The structure of **4a** with atom numbering on ellipsoids drawn at the 50% probability level.

3.2. Pharmacological screening

3.2.1. Cholinesterase inhibitory activities

The newly synthesized triazolothiadiazoles and triazolothiadiazines were assayed for inhibition against EeAChE and hBChE by Ellman's method[40] at micromolar level using neostigmine and donepezil as standard inhibitors. The assay results are summarized in Table 3. Several compounds displayed significant enzyme inhibition. Among them, **5b** of the triazolothiadiazole series was found to be the strongest AChE inhibitor with an IC_{50} value of 3.09 ± 0.154 μM. This compound inhibited AChE~9-fold more strongly than the standard neostigmine, and was approx. twice as effective against AChE as the second standard donepezil (IC_{50} = 7.23 ± 0.12 μM). The strong inhibitory potential for **5b** could be attributed to the electron-donating hydroxyl group present at *para*-position of the aryloxy ring. A slight decrease in activity was observed when the hydroxyl group was replaced by a methyl group in compound **5d** (IC_{50} = 11.3 ± 0.267 μM), but the inhibition was still stronger than of the reference neostigmine. On the other hand, the replacement of aryloxy moiety with heteroaryl rings (pyrrolyl; **4g** and furanyl; **4c**) at 6-position of triazolothiadiazole skeleton reduced the inhibitory activity (IC_{50} 13.7 ± 0.166 and 21.2 ± 0.97 μM, respectively) compared to potent analogues, but inhibition was in the case also still stronger compared to neostigmine. Triazolothiadiazole with a benzyl group at 6-position was found to be less favorable and displayed only 40% inhibition at 100 μM. Similarly, the inhibition was also substantially reduced when a methyl-substituted furanyl group was placed at the same position as revealed by compound **4e**.

On the other hand, in the triazolothiadiazine series, compound **6b** was found to be a potent AChE inhibitor having an IC_{50} value of 15.1 ± 0.213 μM. This inhibitory efficacy might be due to the electron-withdrawing (—Cl) group at the *para*-position of the aryl ring. Comparable inhibitory activity was observed when the chloro group was replaced by another strong electron-deficient (—NO_2) group as revealed by compound **6g** (IC_{50} = 18.3 ± 2.34 μM). When electron-poor groups were replaced with electron-rich groups, reduced activities were observed. Moreover, bulky groups like biphenyl as well as naphthyl were also unfavorable for AChE inhibition. Overall, among the tested compounds, triazolothiadiazoles have displayed stronger AChE inhibition than triazolothiadiazines

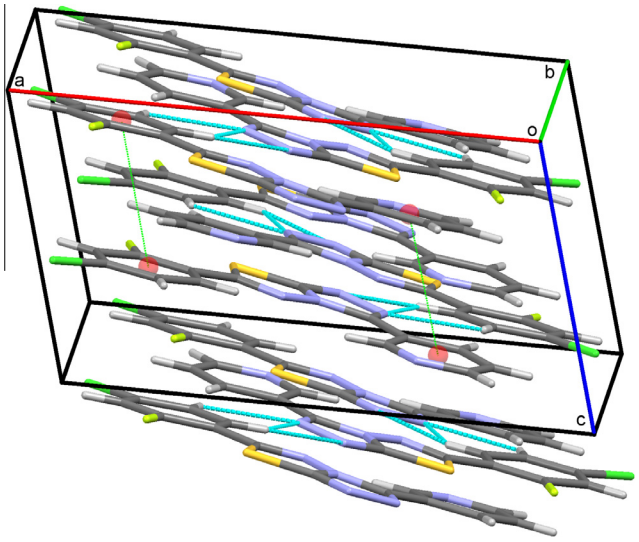

Figure 3. Crystal packing of **4a** viewed along the *b* axis. Hydrogen bonds are shown as dashed lines with representative π…π contacts drawn as dotted lines. Aromatic ring centroids are displayed as colored spheres.

Table 3
AChE and BChE inhibition by compounds **4a–h**, **5a–f** and **6a–h**

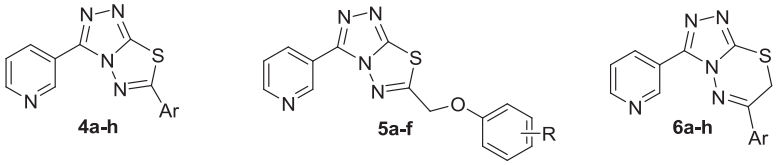

Entry	Ar/R	AChE IC_{50} ± SEM[a] (μM)/%inhibition[b]	BChE IC_{50} ± SEM[a] (μM)/%inhibition[b]
4a	2-F,4-Cl-C_6H_3	(36.2 ± 1.45)[b]	37.4 ± 1.33
4b	3-Cl,4-F-C_6H_3	(48.4 ± 3.78)[b]	10.3 ± 1.15
4c	2-Furanyl	21.2 ± 0.97	6.03 ± 0.551
4d	3-Furanyl	ND	ND
4e	2-CH_3-3-furanyl	37.7 ± 3.21	58.6 ± 0.167
4f	4-F-$C_6H_4CH_2$	(32.3 ± 1.95)[b]	79.9 ± 0.145
4g	2-Pyrrolyl	13.7 ± 0.166	13.7 ± 1.42
4h	4-OC_2H_5-$C_6H_4CH_2$	(38.4 ± 2.34)[b]	70.7 ± 0.156
5a	2-OH	35.5 ± 1.98	3.02 ± 0.58
5b	4-OH	3.09 ± 0.154	0.585 ± 0.154
5c	2-CH_3	ND	ND
5d	4-CH_3	11.3 ± 0.267	4.76 ± 0.323
5e	4-OCH_3	(39.5 ± 2.81)[b]	55.8 ± 2.23
5f	4-F	ND	ND
6a	4-OCH_3-C_6H_4	(15.2 ± 3.2)[b]	0.781 ± 0.213
6b	4-Cl-C_6H_4	15.1 ± 0.213	9.82 ± 0.53
6c	4-F-C_6H_4	(40.8 ± 1.23)[b]	4.92 ± 0.032
6d	4-CH_3-C_6H_4	(28.7 ± 2.13)[b]	25.4 ± 0.84
6e	Biphenyl	39.7 ± 0.211	18.9 ± 0.11
6f	Naphthyl	(17.2 ± 1.97)[b]	15.9 ± 0.11
6g	4-NO_2-C_6H_4	18.3 ± 2.34	1.09 ± 0.156
6h	3,4-Cl_2-C_6H_3	38.5 ± 0.311	64.8 ± 0.123
Neostigmine	—	28.3 ± 2.06	16.3 ± 1.12
Donepezil	—	7.23 ± 0.12	0.02 ± 0.003

ND = not determined.
[a] IC_{50} values represent the concentration of inhibitor required for half-maximal enzyme inhibition and are reported as means of two independent experiments, each performed in triplicate (SEM, standard error of the mean).
[b] % Inhibition at 100 μM.

and should be further considered for the development of novel inhibitors for AD therapy.

The synthesized hybrid compounds were also tested against BChE and eleven compounds were found to possess potent inhibitory activity superior to the standard drug neostigmine. Among them, the 4-hydroxy aryloxy derivative **5b** from the triazolothiadiazole series, was the most potent compound, with IC_{50} = 0.585 ± 0.154 μM. This compound was about 32-fold more potent than neostigmine. The introduction of hydroxyl group at the *ortho*-position of aryloxy ring also resulted in 5-fold higher inhibitory activity than standard inhibitor. Moreover, replacement of the hydroxyl group with a methyl group (**5d**; IC_{50} = 4.76 ± 0.323 μM) led to a small decrease in inhibition but the compound was still 4-fold more active than neostigmine. The presence of a methoxy group at the *para*-position significantly decreased the activity. In the other triazolothiadiazole series (**4a–h**), compound **4c** incorporating a heteroaryl group (furanyl) also inhibited BChE (IC_{50} = 6.03 ± 0.551 μM) twice as strongly as neostigmine. Similarly, the presence of a pyrrolyl group instead of furanyl resulted in slightly higher inhibition (**4g**; IC_{50} = 13.7 ± 1.42 μM). Introduction of halo groups like chloro and fluoro at 3- and 4-position of aryl ring (**4b**; IC_{50} = 10.3 ± 1.15 μM) also displayed significantly enhanced inhibitory activity. In contrast, compounds incorporating substituted heteroaryl and aryl groups (electron-rich and electron-poor) with a methylene linker had diminished activities.

In the triazolothiadiazine series, compounds bearing strong electron-rich (—OMe) and electron-deficient (—NO_2) aryl rings produced remarkable activities. In this case, compound **6a** had an IC_{50} value of 0.781 ± 0.213 μM and was ~23-fold more potent than the reference neostigmine. Similarly, compound **6g** showed 15-fold stronger inhibition of BChE with IC_{50} = 1.09 ± 0.156 μM. Introduction of different halo substituents like fluoro and chloro on the *para*-position of the aryl ring (**6c** and **6b**) exhibited good inhibitory potential with IC_{50} values of 4.92 ± 0.032 and 9.82 ± 0.53 μM, respectively. Compounds with bulky groups like biphenyl (**6e**) and naphthyl (**6f**) possessed inhibitory activity comparable to the reference drug neostigmine. The insertion of another chlorine atom at the *meta*-position of the aryl ring (**6h**), however, resulted in a sharp decrease in inhibition. Overall, displacement of halogen atoms (—Cl and —F) on the aryl group dramatically affected the anti-BChE activity.

In general, among the synthesized hybrid structures, compounds derived from aryloxy acids displayed strong AChE and BChE inhibition. The most active compounds were found to be more potent AChE inhibitors than the two reference drugs neostigmine and donepezil and more potent BChE inhibitors than neostigmine. Considering the strong inhibitory potential of our hybrid compounds, this family of heterocycles holds great promise for the development of new agents for AD therapy.

3.2.2. Cytotoxicity

The synthesized compounds were tested for their cytotoxic potential against lung carcinoma (H157) and vero cell lines in a dose dependent manner using sulforhodamine B (SRB) assays.[42] Vincristine was used as a standard anticancer drug. Vero cells are normal epithelial kidney cells extracted from African green monkey and used here as control to determine the safety. The results of this study are presented in Table 4.

A careful observation of these results (Table 4) revealed that some of the compounds demonstrated promising cytotoxic effects against lung carcinoma (H157) cell lines. Among them, compound **6h** emerged as a potential scaffold for new cytotoxic agents with an IC_{50} value of 0.96 ± 0.43 μM as compared to vincristine (1.03 ± 0.04 μM). This derivative incorporates two chloro substituents on the phenyl ring attached to 6-position of heteroaromatic skeleton. The wide activity range observed for these compounds indicated that the nature of substituents on the aromatic ring at the C-6 position of triazolothiadiazine markedly affects the activity profile of these compounds. Similarly, comparable results were obtained in the triazolothiadiazole series as depicted by compound **4b** incorporating two halogen substituents on phenyl ring attached at C-6 position of basic skeleton. Introduction of other substituents in either series led to the reduction of cytotoxicity as shown by several derivatives like **4a**, **4f**, **5e**, **5f**, **6a**, **6c**, and **6g** with IC_{50} value of 1.95–1.42 μM. On the other hand, all the tested compounds possess low cytotoxicity for normal vero cells.

3.3. Computational binding mode analysis

The X-ray structures of human AChE (PDB ID 4BDT) and BChE (PDB ID 4BDS) were selected for the docking study because electric eel structures for AChE are only available at low crystallographic resolutions (>4 Å) and structures of equine BChE are currently not available. The active site gorge of BChE is considerably larger than the gorge of AChE, which might lead to differences in binding characteristics of dual AChE/BChE inhibitors. Depending on the co-crystallized compounds, different X-ray structures revealed multiple side chain orientations of Tyr337. Therefore, the side chain of Tyr337 in AChE was treated flexibly in our docking study (the corresponding residue Ala328 in BChE has no side chain flexibility).

We have modeled putative binding poses of the best dual AChE/BChE inhibitor **5b** in the active sites of AChE and BChE. In our preferred docking model, the triazolothiadiazole core of the best dual AChE/BChE inhibitor **5b** is located at the bottom of the active site gorge of AChE (Fig. 4, left side). The ring system is in π–π-interaction distance to residue Trp86 and adopts and orientation comparable to the crystallographic inhibitor huprine W. The pyridinyl substituent is directed into a hydrophobic pocket formed by residues Tyr337, Trp439, Pro446, and Tyr449 and might be involved in π–π-interactions with several of those residues, especially with Tyr337. The 4-hydroxy aryloxy moiety of **5b** occupies the mid-gorge area of AChE. The aromatic aryl substructure fits into an aromatic subsite and is surrounded by the aromatic side chains of residues Tyr124, Phe297, Tyr341, Phe388, and Trp286. Furthermore, the hydroxyl group is well positioned for the potential formation of a hydrogen bond to the backbone carbonyl function of residue Arg296.

In the putative binding pose of **5b** within the active site of BChE (Fig. 4, right side), the triazolothiadiazole substructure with the attached pyridinyl substituent closely mimics the predicted pose in AChE and nearly overlaps with crystallographic inhibitor tacrine. The replacement of Phe295 and Phe297 in AChE with the smaller residues Leu286 and Val288 in BChE results in a lower position of the 4-hydroxy aryloxy moiety within the larger mid-gorge area of BChE. The aryl substructure might form π-π-interactions with the side chains of residues Phe329 and Trp231. Again, the 4-hydroxy substituent is well positioned for a hydrogen bonding interaction with the backbone carbonyl group of residue Leu286. For both enzymes, the exchange of the 4-hydroxy moiety (inhibitor **5b**) to a 4-hydroxymethyl substitution (inhibitor **5e**) leads to decrease of activity which might be explained by the loss of the hydrogen bonding interaction to the backbone carbonyls of residues Arg296 (AChE) and Leu286 (BChE).

In summary, plausible binding conformations could be generated for the best dual inhibitor **5b** in AChE and BChE that are thought to rationalize the comparable potency of this compound against both enzymes.

Table 4
Cytotoxic potential of synthesized compounds **4a–h**, **5a–f** and **6a–h**

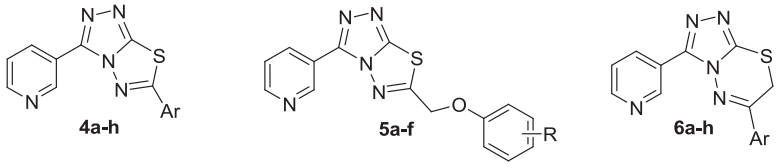

Entry	Ar/R	Lung carcinoma (H157) cell lines IC_{50} ± SEM (μM)	Vero cell lines cytotoxicity (%)
4a	2-F,4-Cl-C_6H_3	1.87 ± 0.21	26.7 ± 3.15
4b	3-Cl,4-F-C_6H_3	1.08 ± 0.04	23.6 ± 4.09
4c	2-Furanyl	3.16 ± 0.82	23.9 ± 2.10
4d	3-Furanyl	3.41 ± 0.34	28.4 ± 2.01
4e	2-CH_3-3-furanyl	2.93 ± 0.71	24.3 ± 1.28
4f	4-F-$C_6H_4CH_2$	1.65 ± 0.19	21.3 ± 3.14
4g	2-Pyrrolyl	5.14 ± 1.02	19.2 ± 1.42
4h	4-OC_2H_5-$C_6H_4CH_2$	2.92 ± 0.34	22.5 ± 2.11
5a	2-OH	3.67 ± 0.41	22.7 ± 1.35
5b	4-OH	3.01 ± 0.01	20.4 ± 4.53
5c	2-CH_3	3.29 ± 1.14	20.9 ± 3.44
5d	4-CH_3	2.98 ± 0.61	23.8 ± 2.19
5e	4-OCH_3	1.95 ± 0.02	24.1 ± 3.47
5f	4-F	1.94 ± 0.02	17.4 ± 3.24
6a	4-OCH_3-C_6H_4	1.67 ± 0.84	27.8 ± 2.02
6b	4-Cl-C_6H_{4w}	3.94 ± 0.74	21.1 ± 3.47
6c	4-F-C_6H_4	1.85 ± 0.43	18.4 ± 2.28
6d	4-CH_3-C_6H_4	3.87 ± 0.52	27.3 ± 3.61
6e	Biphenyl	4.32 ± 1.02	26.1 ± 2.43
6f	Naphthyl	5.37 ± 0.98	23.1 ± 2.53
6g	4-NO_2-C_6H_4	1.42 ± 0.86	10.7 ± 3.18
6h	3,4-Cl_2-C_6H_3	0.96 ± 0.43	22.2 ± 5.16
Vincristine	—	1.03 ± 0.04	16.81 ± 1.15

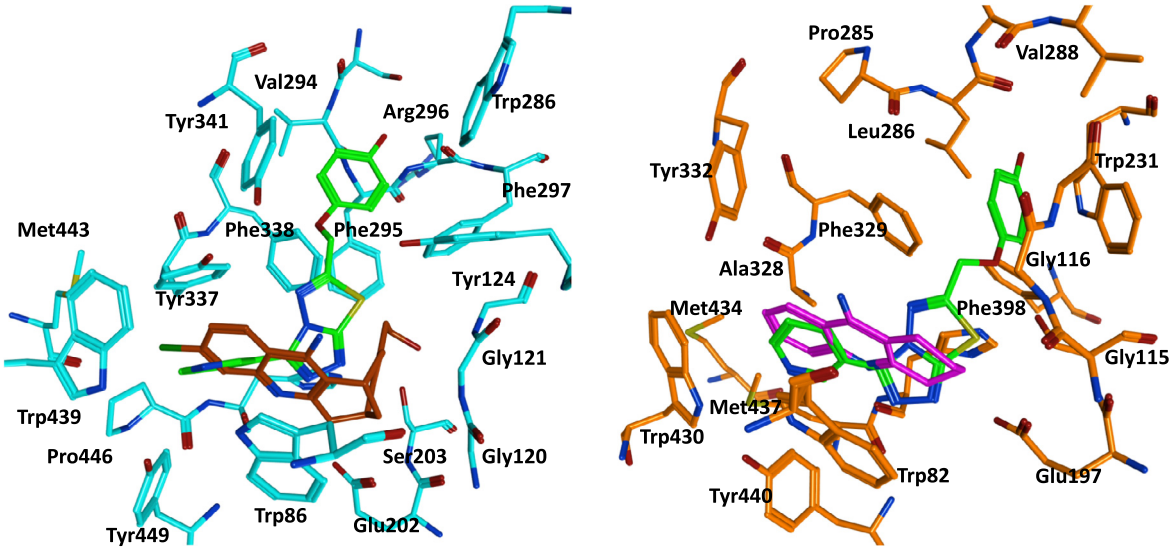

Figure 4. Binding mode predictions. On the left, an overlay of the predicted binding mode of inhibitor **5b** (carbon atoms colored green) and the crystallographic inhibitor huprine W (carbon atoms colored brown) in the active site of AChE (cyan) is shown. On the right, and overlay of the putative binding conformation of compound **5b** (carbon atoms colored green) and crystallographic inhibitor tacrine (carbon atoms colored magenta) in the active site of BChE (orange) is shown.

4. Conclusions

In this study, 22 novel derivatives of triazolothiadiazoles and triazolothiadiazines were designed, synthesized and characterized by spectro-analytical methods and, in case of **4a**, by X-ray crystallography. In addition, plausible binding modes of the best dual inhibitor were modeled. The synthetic pathway was effective providing title compounds in good yields. Structural diversity of the final compounds was ensured by using a range of substituted aromatic/heteroaromatic/aryloxy acids and phenacyl bromides. All the synthetic compounds were evaluated for their ability to inhibit AChE and BChE. The anticholinesterase activities were compared to those of neostigmine and donepezil as standards. Among the evaluated hybrids, several compounds were identified as potent inhibitors. Compounds **5b** and **5d** exhibited strongest AChE inhibition with IC_{50} values of 3.09 ± 0.154 and 11.3 ± 0.267 μM, respectively, whereas **5b**, **6a** and **6g** were most potent inhibitors against BChE with IC_{50} values of 0.585 ± 0.154, 0.781 ± 0.213, and 1.09 ± 0.156 μM, respectively, compared to standard drug neostigmine (28.03 ± 2.06 and 16.3 ± 1.12 μM). Taken together, our results indicate that the newly identified AChE and BChE inhibitors should merit further consideration as templates for the development of novel compounds for AD therapy. The compounds were also tested for their cytotoxic effects against lung carcinoma (H157) and vero cell lines. Among them, compound **6h** emerged as a potential scaffold for new cytotoxic agents with an IC_{50} value of 0.96 ± 0.43 μM as compared to standard drug vincristine (1.03 ± 0.04 μM).

Acknowledgments

We thank the University of Otago for purchase of the diffractometer. N.F. is supported by a fellowship from the Jürgen Manchot Foundation, Düsseldorf, Germany.

Supplementary data

CCDC 994768 contains the supplementary crystallographic data for this paper. These data can be obtained free of charge from The Cambridge Crystallographic Data Centre via http://www.ccdc.cam.ac.uk/data_request/cif. Supplementary data related to this article can be found with the online version of the paper.

Supplementary data associated with this article can be found, in the online version, at http://dx.doi.org/10.1016/j.bmc.2014.08.026.

References and notes

1. Bartolucci, C.; Perola, E.; Pilger, C.; Fels, G.; Lambal, D. *Proteins* **2001**, *42*, 182.
2. Klafki, H.; Staufenbiel, M.; Kornhuber, J.; Wiltfang, J. *Brain* **2006**, *129*, 2840.
3. Edwards, P. D.; Albert, J. S.; Sylvester, M.; Aharony, D.; Andisik, D.; Callaghan, O.; Campbell, J. B.; Carr, R. A.; Chessari, G.; Congreve, M.; Frederickson, M.; Folmer, R. H. A.; Geschwindner, S.; Koether, G.; Kolmodin, K.; Krumrine, J.; Mauger, R. C.; Murray, C. W.; Olsson, L.; Patel, S.; Spear, N.; Tian, G. *J. Med. Chem.* **2007**, *50*, 5912.
4. Ferri, C. P.; Prince, M.; Brayne, C.; Brodaty, H.; Fratiglioni, L.; Ganguli, M.; Hall, K.; Hasegawa, K.; Hendrie, H.; Huang, Y.; Jorm, A.; Mathers, C.; Menezes, P. R.; Rimmer, E.; Scazufca, M. *Lancet* **2005**, *366*, 2112.
5. Cho, Y.-S.; Kim, S.-K.; Ahn, C.-B.; Je, J.-Y. *Carbohydr. Polym.* **2011**, *84*, 690.
6. Karlsson, D.; Fallarero, A.; Brunhofer, G.; Mayer, C.; Prakash, O.; Mohan, C. G.; Vuorela, P.; Erker, T. *Eur. J. Pharm. Sci.* **2012**, *47*, 190.
7. Gibney, G.; Camp, S.; Dionne, M.; MacPhee-Quigley, K.; Taylor, P. *Proc. Natl. Acad. Sci. U.S.A.* **1990**, *87*, 7546.
8. Ekholm, M.; Konschin, H. *J. Mol. Struct: Theochem* **1999**, *467*, 161.
9. Ordentlich, A.; Barak, D.; Kronman, C.; Ariel, N.; Segall, Y.; Velan, B.; Shafferman, A. *J. Biol. Chem.* **1998**, *273*, 19509.
10. Vellom, D. C.; Radic, Z.; Li, Y.; Pickering, N. A.; Camp, S.; Taylor, P. *Biochemistry* **1993**, *32*, 12.
11. Taylor, P.; Lappi, S. *Biochemistry* **1975**, *14*, 1989.
12. Barak, D.; Kronman, C.; Ordentlich, A.; Ariel, N.; Bromberg, A.; Marcus, D.; Lazar, A.; Velan, B.; Shafferman, A. *J. Biol. Chem.* **1994**, *269*, 6296.
13. Bartus, R.; Dean, R. R.; Beer, B.; Lippa, A. *Science* **1982**, *217*, 408.
14. Musiał, A.; Bajda, M.; Malawska, B. *Curr. Med. Chem.* **2007**, *14*, 2654.
15. Yu, Q.; Holloway, H. W.; Flippen-Anderson, J. L.; Hoffman, B.; Brossi, A.; Greig, N. H. *J. Med. Chem.* **2001**, *44*, 4062.
16. Rizzo, S.; Rivière, C.; Piazzi, L.; Bisi, A.; Gobbi, S.; Bartolini, M.; Andrisano, V.; Morroni, F.; Tarozzi, A.; Monti, J. P.; Rampa, A. *J. Med. Chem.* **2008**, *51*, 2883.
17. Saxena, A.; Redman, A. M.; Jiang, X.; Lockridge, O.; Doctor, B. P. *Biochemistry* **1997**, *36*, 14642.
18. Elsinghorst, P. W.; Gonzales Tanarro, C. M.; Gütschow, M. *J. Med. Chem.* **2006**, *49*, 7540.
19. Darvesh, S.; McDonald, R. S.; Darvesh, K. V.; Mataija, D.; Conrad, S.; Gomez, J.; Walsh, R.; Martin, E. *Bioorg. Med. Chem.* **2007**, *15*, 6367.
20. Shaker, R. M. *ARKIVOC* **2006**, *ix*, 59.
21. Purohit, D. H.; Dodiya, B. L.; Ghetya, R. M.; Vekariya, P. B.; Joshi, H. S. *Acta Chim. Slov.* **2011**, *58*, 53.
22. Varvaresou, A.; Siatra-Papastaikoudi, T.; Trotinis, A.; Tsantili-Kakoulidou, A.; Vamvakides, A. *Farmaco* **1998**, *53*, 320.
23. Kaplancikli, Z. A.; Turan-Zitouni, G.; Oezdemir, A.; Revial, G. *Eur. J. Med. Chem.* **2008**, *43*, 155.
24. Foroumadi, A.; Mirzaei, A.; Shafiee, A. *Pharmazie* **2001**, *56*, 610.
25. Chen, H.; Li, Z.; Han, Y. *J. Agric. Food Chem.* **2000**, *48*, 5312.
26. Ammar, Y. A.; Ghorab, M. M.; El-Sharief, A. M. S.; Mohamed, S. I. *Heteroat. Chem.* **2002**, *13*, 199.
27. Heindel, N. D.; Reid, J. R. *J. Heterocycl. Chem.* **1980**, *17*, 1087.

28. Boschelli, D. H.; Connor, D. T.; Kostlan, C. R.; Kramer, J. B.; Mullican, M. D.; Sircar, J. C. U.S. Patent 5,102,897, A, **1992**.
29. Kamal, A.; Khan, M. N. A.; Srikanth, Y. V. V.; Reddy, K. S.; Juvekar, A.; Sen, S.; Kurian, N.; Zingde, S. *Bioorg. Med. Chem.* **2008**, *16*, 7804.
30. Skoumbourdis, A. P.; LeClair, C. A.; Stefan, E.; Turjanski, A. G.; Maguire, W.; Titus, S. A.; Huang, R.; Auld, D. S.; Inglese, J.; Austin, C. P.; Michnick, S. W.; Xia, M.; Thomas, C. J. *Bioorg. Med. Chem. Lett.* **2009**, *19*, 3686.
31. Lauffer, D.; Li, P.; Mcginty, K. U.S. Patent 8,269,012, B2, **2012**.
32. El-Shehry, M. F.; Abu-Hashem, A. A.; El-Telbani, E. M. *Eur. J. Med. Chem.* **2010**, *45*, 1906.
33. Zhang, L. X.; Zhang, A. J.; Chen, X. X.; Lei, X. X.; Nan, X. Y.; Chen, D. Y.; Zhang, Z. Y. *Molecules* **2002**, *7*, 681.
34. Rafiq, M.; Saleem, M.; Hanif, M.; Maqsood, M. R.; Rama, N. H.; Lee, K.-H.; Seo, S.-Y. *Bull. Korean Chem. Soc.* **2012**, *33*, 3943.
35. Khan, I.; Zaib, S.; Ibrar, A.; Rama, N. H.; Simpson, J.; Iqbal, J. *Eur. J. Med. Chem.* **2014**, *78*, 167.
36. Khan, I.; Ali, S.; Hameed, S.; Rama, N. H.; Hussain, M. T.; Wadood, A.; Uddin, R.; Ul-Haq, Z.; Khan, A.; Ali, S.; Choudhary, M. I. *Eur. J. Med. Chem.* **2010**, *45*, 5200.
37. Eweiss, N. F.; Bahajaj, A. A.; Elsherbini, E. A. *J. Heterocycl. Chem.* **1986**, *23*, 1451.
38. Almajan, G. L.; Barbuceanu, S. F.; Saramet, I.; Draghici, C. *Eur. J. Med. Chem.* **2010**, *45*, 3191.
39. Lei, X.; Zhang, L.; Zhang, A.; Ye, X.; Xiong, J. *Magn. Reson. Chem.* **2007**, *45*, 265.
40. Ellman, G. L.; Courtney, K. D.; Andres, V., Jr; Feather-Stone, R. M. *Biochem. Pharmacol.* **1961**, *7*, 88.
41. Araki-Sasaki, K.; Aizawa, S.; Hiramoto, M.; Nakamura, M.; Iwase, O.; Nakata, K.; Sasaki, Y.; Mano, T.; Handa, H.; Tano, Y. *J. Cell Physiol.* **2000**, *182*, 189.
42. Skehan, P.; Storeng, R.; Scudiero, D.; Monks, A.; McMahon, J.; Vistica, D.; Warren, J. T.; Bokesch, H.; Kenney, S.; Boyd, M. R. *J. Natl. Cancer Inst.* **1990**, *82*, 1107.
43. Longo-Sorbello, G. S.; Say, G. m.; Banerjee, D.; Bertino, J. R. Cytotoxicity and Cell Growth Assays, in: Cell Biology, Four-Volume Set: a Laboratory Handbook, vol. 1, 2005, p. 315.
44. APEX2, SAINT and SADABS. Bruker AXS Inc., Madison, Wisconsin, USA 2011.
45. Sheldrick, G. M. *Acta Crystallogr. A.* **2008**, *64*, 112.
46. Hunter, K. A.; Simpson, J. A. *TITAN 2000*; University of Otago: New Zealand, 1999.
47. Macrae, C. F.; Bruno, I. J.; Chisholm, J. A.; Edgington, P. R.; McCabe, P.; Pidcock, E.; Rodriguez-Monge, L.; Taylor, R.; van de Streek, J.; Wood, P. A. *J. Appl. Cryst.* **2008**, *41*, 466.
48. Nachon, F.; Carletti, E.; Ronco, C.; Trovaslet, M.; Nicolet, Y.; Jean, L.; Renard, P.-Y. *Biochem. J.* **2013**, *453*, 393.
49. *RCSB Protein Data Bank*. http://www.rcsb.org.
50. Morris, G. M.; Huey, R.; Lindstrom, W.; Sanner, M. F.; Belew, R. K.; Goodsell, D. S.; Olson, A. J. *J. Comput. Chem.* **2009**, *30*, 2785.
51. Molecular Operating Environment (MOE), 2012.10; Chemical Computing Group Inc., 1010 Sherbooke St. West, Suite #910, Montreal, QC, Canada, H3A 2R7; 2012.
52. Allen, F. H. *Acta Crystallogr. B.* **2002**, *58*, 380.